PLASMONICS

Asymmetric excitation of surface plasmons by dark mode coupling

10.1126/sciadv.1501142

Xueqian Zhang,[1]* Quan Xu,[1]* Quan Li,[1] Yuehong Xu,[1] Jianqiang Gu,[1] Zhen Tian,[1] Chunmei Ouyang,[1] Yongmin Liu,[2] Shuang Zhang,[3] Xixiang Zhang,[4] Jiaguang Han,[1†] Weili Zhang[1,5†]

Control over surface plasmons (SPs) is essential in a variety of cutting-edge applications, such as highly integrated photonic signal processing systems, deep-subwavelength lasing, high-resolution imaging, and ultrasensitive biomedical detection. Recently, asymmetric excitation of SPs has attracted enormous interest. In free space, the analog of electromagnetically induced transparency (EIT) in metamaterials has been widely investigated to uniquely manipulate the electromagnetic waves. In the near field, we show that the dark mode coupling mechanism of the classical EIT effect enables an exotic and straightforward excitation of SPs in a metasurface system. This leads to not only resonant excitation of asymmetric SPs but also controllable exotic SP focusing by the use of the Huygens-Fresnel principle. Our experimental findings manifest the potential of developing plasmonic metadevices with unique functionalities.

INTRODUCTION

The common motivation in realizing the electromagnetically induced transparency (EIT) effect in metamaterial systems is to deliver a sharp transmission resonance that can slow down light (*1*). To achieve this, the design generally consists of two artificial resonant elements, a radiative bright resonator that strongly couples with the light in free space and a dark resonator that weakly couples to the incident light (*2*–*12*). These artificial structures thus have EIT-like resonances due to near-field Fano-type destructive interference (*13*–*16*). Therein, the dispersion property of the coupled system is markedly modified, leading to an enhanced group refractive index around the transparency window. Such a behavior renders the metamaterial-based EIT effect very promising in optical switching, sensing, slow light, light storage, and enhanced nonlinear effects (*9*–*12*, *17*–*20*).

Although a series of micro- and nanostructures have been developed to demonstrate the EIT effect, the strategies investigated thus far mostly involve manipulating the electromagnetic waves in free space (*2*–*20*) or plasmonic waveguides using cavity structures and antennas (*21*–*23*). However, it is expected that the unique mode coupling mechanism of the EIT effect could be used to control not only the electromagnetic waves propagating in free space and waveguides but also surface plasmons (SPs) existing at the near-field metal-dielectric interface (*24*). The ever-increasing demands for functional plasmonic devices have driven great efforts to exploit new methods for excitation and manipulation of SPs, especially for asymmetric or unidirectional excitation of SPs. Among these, one approach is to use metasurfaces with controllable phase profiles (*25*–*32*), where the designed phase gradient serves as an additional in-plane wave vector that is critical to satisfy the momentum-matching condition between the free-space wave and SPs in a selective excitation direction (*33*–*35*). Another route is to control the SP interference by two or more isolated couplers with different SP excitation phases or scattering parameters, including previously reported compact asymmetric gratings and plasmonic antenna couplers (*36*–*42*). However, to achieve the desired functionality with high performance, simplifications were usually made where freedoms in controlling the SPs were also missed at the same time. For example, the coupling effects among the excitation units have been purposely excluded or minimized in previous studies. Instead, coupling can also be an essential factor in designing the SP excitation and cannot be neglected in many applications. New designs for much improved control over the SPs may be achieved by investigating the sophisticated coupling mechanism, such as EIT, within the building block.

Here, we apply the EIT mode coupling mechanism to the near-field SPs, enabling a new degree of freedom in controlling the excitation and propagation of the SP resonance. We show that the resonance strength of the bright resonator, which determines the strength of the excited SP along a specific direction, can be suppressed strongly at one side when coupled with the dark resonator. Once stimulated, the dark resonator excites a new orthogonally propagating SP resonance. Both the intensities of these two SP beams can be effectively manipulated by varying the coupling between the two sets of resonators. Different from previous studies on the asymmetric excitation where the far-field interference of the scattered SP fields played an essential role, here, the near-field coupling–induced destructive mode interference is responsible for the asymmetric response. In addition, we demonstrate that the proposed method can be further used to achieve an exotic SP focusing by simply applying the Huygens-Fresnel principle (*43*, *44*). The unique property of our strategy delivers a versatile platform for various applications in asymmetric SP excitations, plasmonic circuitry, and energy harvesting.

RESULTS

Sample design and terahertz near-field characterization

The proposed design of the subwavelength unit cell is schematically illustrated in Fig. 1A. The structure contains a bar-shape slit resonator (BSSR) and a split-ring slit resonator (SRSR) at the lower right side of

[1]Center for Terahertz Waves, College of Precision Instrument and Optoelectronics Engineering, and the Key Laboratory of Optoelectronics Information and Technology (Ministry of Education), Tianjin University, Tianjin 300072, China. [2]Department of Mechanical and Industrial Engineering, Northeastern University, Boston, MA 02115, USA. [3]School of Physics and Astronomy, University of Birmingham, Birmingham B15 2TT, UK. [4]Division of Physical Science and Engineering, King Abdullah University of Science and Technology, Thuwal 23955-6900, Saudi Arabia. [5]School of Electrical and Computer Engineering, Oklahoma State University, Stillwater, OK 74078, USA.
*These authors contributed equally to this work.
†Corresponding author. E-mail: jiaghan@tju.edu.cn (J.H.); weili.zhang@okstate.edu (W.Z.)

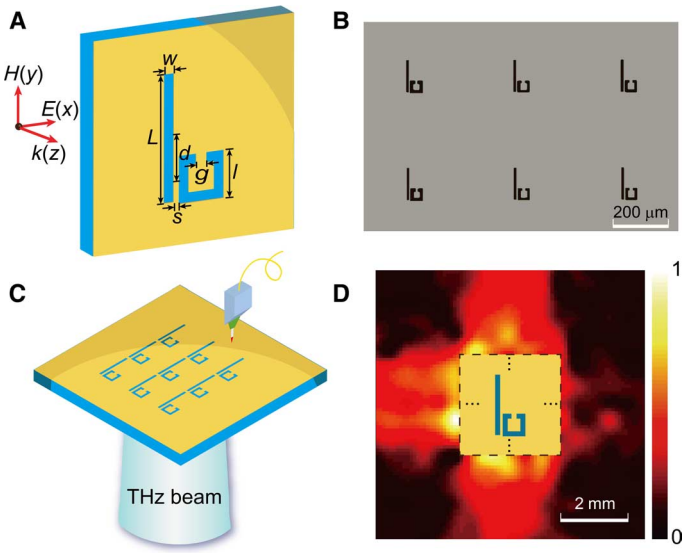

Fig. 1. Sample design, experimental diagram, and measured field distribution. (**A**) Schematic view of a unit cell of the metallic hole-type structure. The geometric parameters are as follows: L = 120 μm, w = 10 μm, l = 45 μm, g = 10 μm, d = −40 μm, and s = 5 μm. (**B**) Microscope image of a part of the fabricated metasurface. (**C**) Experimental schematic of the terahertz near-field mapping measurement of the metasurface. (**D**) Measured electric field (E_z) distribution of the excited terahertz SP amplitude at 0.75 THz under normal incidence of an x-polarized wave, where 8 × 8 unit cells were contained and arranged in a square lattice. The inset schematically shows the excitation pattern.

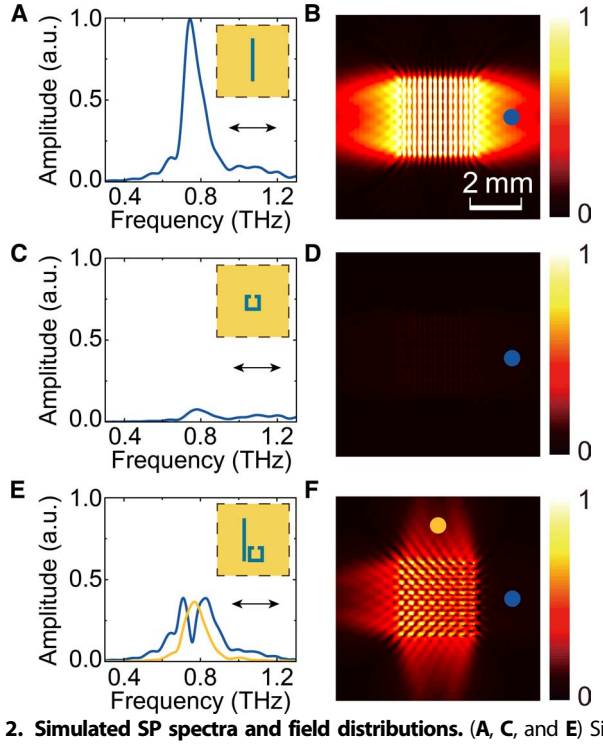

Fig. 2. Simulated SP spectra and field distributions. (**A**, **C**, and **E**) Simulated SP amplitude spectra of the 8 × 8 unit cells of BSSR, SRSR, and combination of BSSR and SRSR under the x-polarization incidences, respectively, as indicated by the insets and arrows. (**B**, **D**, and **F**) Corresponding (on the same row) simulated amplitude field (E_z) distributions of the excited terahertz SPs of BSSR, SRSR, and combination of BSSR and SRSR under the x-polarization incidences at 0.75 THz, respectively. The blue (3-mm distance to the center along the +x direction) and orange (3-mm distance to the center along the +y direction) circles in (B), (D), and (F) represent the positions where the spectra in (A), (C), and (E) were extracted, and the colors of the circles indicate the curves with the same colors. a.u., arbitrary unit.

the BSSR. The resonance frequency of the structure is designed at 0.75 THz, where the SPs can be excited most efficiently. To increase the overall SP coupling strength at the resonance, we fabricated a metasurface with 8 × 8 such unit cells made from aluminum on a quartz substrate using conventional photolithography. In the terahertz range, because most metals function closely as perfect electric conductors with permittivity $|\varepsilon_m| \gg 1$, the dispersion relation of the SP is very close to that of the free-space wave

$$k_{SP} = k_0\sqrt{\varepsilon_m/(\varepsilon_m + 1)} \approx k_0$$

with k_{SP} and k_0 being the SP and free-space wave numbers, respectively (*45*–*49*). Here, the periodicity of the metasurface was set to be 400 μm along both the x and y directions so that the excited SPs from each structure on the air side can interfere constructively with each other in the far-field region of the SPs. Figure 1B shows the microscopic image of a part of the fabricated sample.

To map the SP field distribution, a nearly uniform terahertz beam was normally illuminating on the metasurface from the substrate side, and a fiber-coupled near-field terahertz microprobe was used to scan the SP field (see Fig. 1C and Materials and Methods) (*50*). The incident terahertz beam was collimated with a spot size of 5-mm diameter, which is large enough to cover the whole excitation area (3.2 × 3.2 mm^2). The polarization was set to be along the x direction using a metallic grid polarizer to ensure the excitation of BSSRs. Driven by a two-dimensional (2D) translation stage, the microprobe raster scans the SP field over a large area. To allow the detected terahertz pulse to be long enough to cover the entire pulse duration, a 2-mm-thick quartz wafer (ε_q = 3.76) was used as the substrate to avoid Fabry-Perot reflections within 26 ps after the main terahertz pulse.

The measured SP field distribution is illustrated in Fig. 1D, in which the inset schematically shows the excitation structure and its actual area. An asymmetric SP excitation pattern is clearly observed along the x direction. That is, the SPs mainly propagate toward the left side (−x direction) of the structure, whereas there are almost no SPs on the right side (+x direction). Another intriguing effect is that an x-polarized wave is also coupled to the y direction propagating SPs with nearly the same strength on both the top side (+y direction) and the bottom side (−y direction). It is known that the SP propagating at a metal-dielectric interface is actually an electron density wave, which only exists as a transverse magnetic mode. This oscillation of electrons is driven by the electric field of the incident wave; thus, the propagating direction of the SPs is usually locked to be along the wave polarization at normal incidence. However, now, we can obtain SPs propagating along the y axis, although the incident light is x-polarized. Through analyses presented in the following, we find that the effect can be well explained by the EIT coupling theory.

Theoretical analysis

To explore the underlying physical mechanism of the phenomena, we first individually analyzed the SP responses of the two resonators

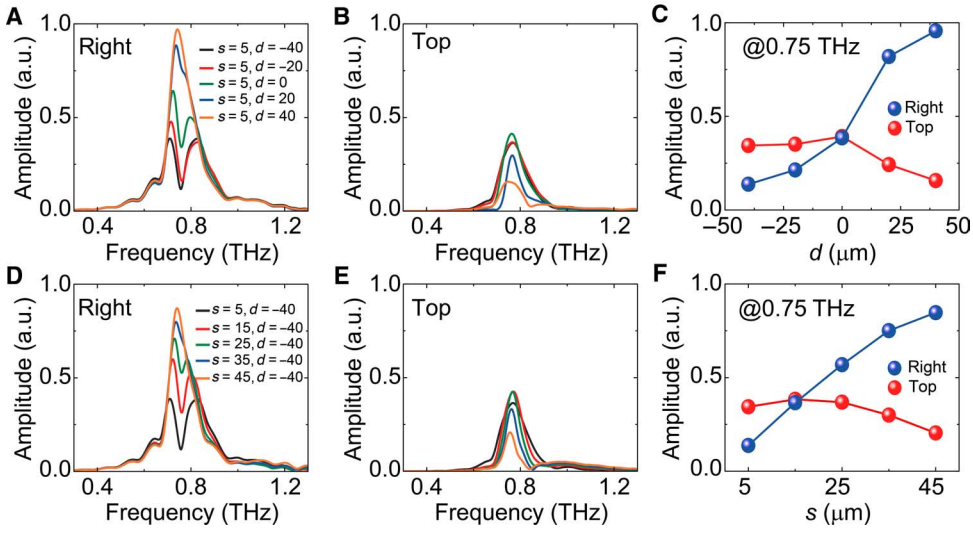

Fig. 3. Simulated spectrum variations with different values of *d* and *s*. (**A** and **B**) Simulated SP amplitude spectra excited to the right and top sides (blue and orange points in Fig. 2) of the structures, with *d* varying from −40 to 40 μm and *s* = 5 μm. (**C**) Variations of the SP amplitude at 0.75 THz excited to the right and top sides of the structures with respect to *d*. (**D** and **E**) Simulated SP amplitude spectra excited to the right and top sides of the structures, with *s* varying from 5 to 45 μm and *d* = −40 μm. (**F**) Variations of the SP amplitude at 0.75 THz excited to the right and top sides of the structures with respect to *s*.

(BSSR and SRSR). Here, the commercially available software package CST Microwave Studio was used to simulate the spectrum and field distribution of the excited SPs (see Materials and Methods). For BSSR, the strength of the excited SPs becomes strongest when the incident polarization is perpendicular to the longer side of the slit. Figure 2A illustrates the normalized SP spectrum excited from BSSR array under the *x*-polarization incidence, as indicated in the inset. The excited SPs are resonating at 0.75 THz. The corresponding SP field distribution at 0.75 THz is shown in Fig. 2B. It can be seen that the SPs are only excited along the *x* direction, whereas there are no SPs along the *y* direction. As for SRSR, the SPs can hardly be excited under the *x*-polarization incidence (Fig. 2, C and D). To this end, the SPs excited by the individual resonator arrays are all symmetric and propagate along the polarization direction.

The situation is changed when these two resonators are coupled together. Figure 2E shows that a sharp SP excitation dip is induced among the peak of the BSSR array at 0.75 THz, splitting the original peak into two smaller ones. Meanwhile, the newly generated SPs along the ±*y* direction appear and resonate at 0.75 THz. Note that they cannot be excited when there is only one type of resonator under the *x*-polarization incidence. Figure 2F illustrates the simulated SP field distribution at 0.75 THz, which is in very good agreement with the experimental result (Fig. 1D). Such an intriguing behavior is quite similar to the EIT effect where the newly generated SPs along the ±*y* directions correspond to the EIT transparency window and the weakened SPs along the +*x* direction correspond to the suppression of the bright resonator. In this case, BSSR with strong and broadband response and SRSR with weak and narrow response function as the bright resonator and dark resonator, respectively. Once the BSSR is excited by the incident *x*-polarized wave, it strongly couples to the SRSR. Then, the SRSR will excite its own SPs along the ±*y* directions with the same strength (see fig. S1). Because SRSR is only located at the right side of BSSR, the SP intensity at the right side of the BSSR is strongly suppressed. The scattered field of the SPs arisen from the destructive interference effect leads to the disappearance of the right-side SPs. In contrast, the SP intensity at the left side is less affected by the SRSR (see figs. S2 and S3). Here, we only focus on the SP excitation along the top/bottom and right sides of the structure.

One important feature of the EIT effect is that the transparency window can be gradually adjusted by changing the coupling strength κ between the bright and dark resonators. The same strategy can be applied to control the SP intensity along the +*x* and ±*y* directions. This can be described by applying the coupled Lorentzian oscillator model, through which the resonance amplitude of the resonators with respect to κ can be solved (see note S1). It can be deduced that the resonance amplitude of the bright resonator gradually increases to approach that of a single bright resonator as κ decreases, whereas the resonance amplitude of the dark resonator does not change monotonically with κ and a maximum of the resonance amplitude of the dark resonator can be found when κ changes. Such a behavior will directly transfer to that of the excited SP intensity, which is strongly dependent on the resonance amplitude of the resonators.

Numerical simulations and experimental verification

There are two approaches to change the coupling coefficient: varying the relative vertical distance *d* or horizontal distance *s* between the two resonators. Figure 3 (A and B) illustrates the change of the SP amplitude spectra with respect to *d* at the right and top sides of the structure, respectively. As *d* varies from −40 to 40 μm (*s* is kept at 5 μm), the SP excitation dip on the right side is gradually converted to one peak, whereas the SP excitation peak on the top side rises first and then decreases. Such variations are more clearly shown in Fig. 3C at 0.75 THz. Similar modulation of the SP excitation amplitudes is also observed as *s* varies from 5 to 45 μm (*d* is kept at −40 μm; see Fig. 3, D to F). The variation of the SP amplitude spectra at the left and bottom sides of the structure can be seen in fig. S3.

To identify how the coupling coefficient changes with these two parameters, we look into the electric and magnetic coupling regimes between BSSR and SRSR. For the well-known split-ring resonator (SRR), it can be excited by either an electric field perpendicular to

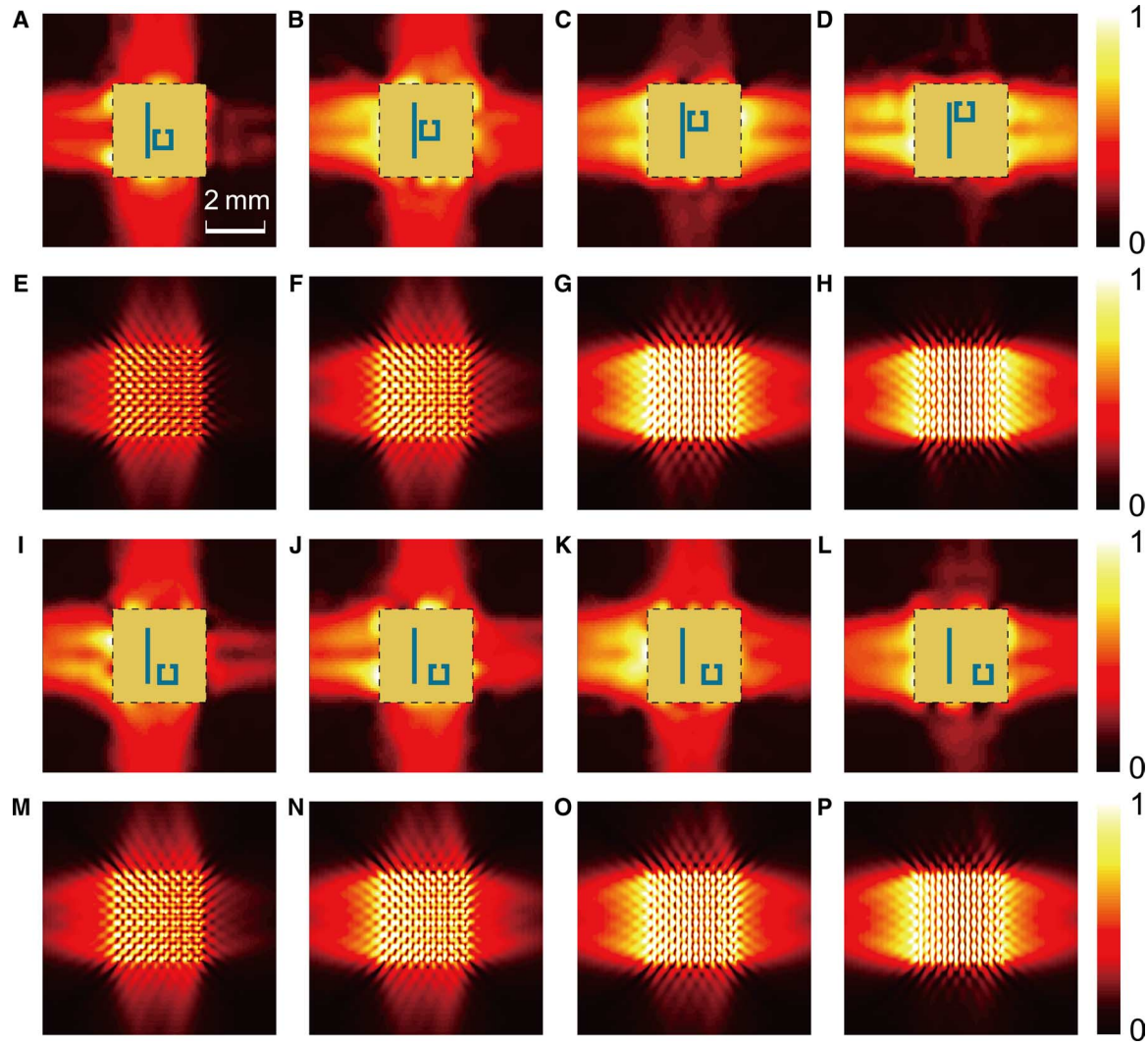

Fig. 4. Measured and simulated SP amplitude distributions. (**A** to **D**) Measured SP amplitude distributions, with d varying from −20 to 40 μm and s = 5 μm at 0.75 THz. The insets schematically show the measured structures. (**E** to **H**) Simulated SP amplitude distributions corresponding to (A) to (D), respectively. (**I** to **L**) Measured SP amplitude distributions, with s varying from 5 to 45 μm and d = −40 μm at 0.75 THz. The insets schematically show the measured structures. (**M** to **P**) Simulated SP amplitude distributions corresponding to (I) to (L), respectively.

the gap E_x or a magnetic field passing through the ring H_z. On the contrary, SRSR can be excited by a magnetic field perpendicular to the gap H_x or an electric field passing through the ring E_z according to the Babinet principle (*51*–*53*). From simulations, we found that the localized electric field E_z of an excited BSSR is strongest at the center whereas the localized magnetic field H_x is strongest around the ends of BSSR but in opposite phase (see fig. S2). At s = 5 μm, the electric and magnetic couplings from BSSR to SRSR are in phase when d = −40 μm, resulting in maximum excitation of the SRSR. As SRSR is gradually moved to d = 40 μm, the electric and magnetic couplings to the SRSR become out of phase, and so, SRSR is hardly excited. Therefore, the overall coupling coefficient decreases with d increasing. As for the case of increasing the coupling distance s, both the electric and magnetic couplings decrease, and hence, the overall coupling coefficient also decreases.

Notice that such a coupling mechanism is strongly related to the direction of SRSR. If the SRSR is flipped up and down with respect to its own center, the overall coupling coefficient increases with increasing d, as the structure becomes its mirror structure along the y direction (see fig. S4A). To explore the specific effects of the electric and magnetic couplings in this process, we could achieve further in-depth understanding by analyzing the complementary structure of the design, which consists of a bar-shape resonator (BSR) and SRR (*8*). As an example, we consider a case of flipping the SRR at d = 40 μm where the overall coupling is quite weak (see fig. S4B). First, the magnetic coupling effect from the H_z resonant field of BSR to SRR persists, because it penetrates the SRR and causes an inductive surface current, which circulates along the SRR in a certain direction regardless of the direction of SRR. However, the electric coupling effect from the E_x resonant field of BSR to SRR is different. Because the coupling field E_x from BSR will strongly attract or repel the free electrons at the nearest edge of SRR, whereas it has a less effect on the other edge of SRR due to asymmetric E_x environment caused by the distance (*7*); such behavior will also cause a circulating surface current along the SRR. The difference is the fact that the circulating direction will reverse

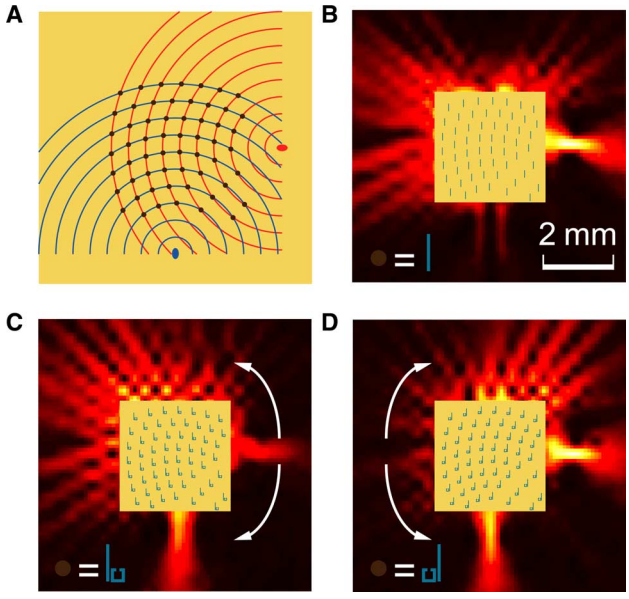

Fig. 5. Schematic of the SP focusing structure and measured results. (**A**) Schematic illustrating of the unit cell arrangment of the designed structure. The brown points indicate the locations of the unit cells. The blue and red elliptical points are the designed focuses. Both the maximum and minimum radii of the blue and red circles are 400 and 4000 μm, respectively. (**B** to **D**) Measured SP amplitude distributions when the arranged unit cell was BSSR, BSSR with SRSR at its right side and left side of $d = -40$ μm and $s = 5$ μm at 0.75 THz, respectively, as indicated by the corresponding insets. The arrows indicate the pathways of the SP energy conversion.

when the SRR is flipped. In our case, before flipping the SRR, the magnetic and electric coupling–induced surface currents are circulating along the SRR out of phase, so they cancel each other out, and the overall coupling markedly decreases. After the SRR is flipped, the induced surface currents are circulating in phase, and the overall coupling is enhanced (see fig. S4, C and D). Such a process is also true for the other values of d and s. The proposed hole-type structures here undergo a similar coupling process but with the E_z and H_x coupling fields instead.

To verify the theory and simulations, terahertz SP near-field mapping was carried out on various samples with different values of d and s. Figure 4 (A to D) illustrates the experimental results of the SP amplitude distributions at 0.75 THz when $s = 5$ μm and $d = -20$, 0, 20, and 40 μm, respectively. The SP amplitude changes on the four sides (left, right, top, and bottom) of the structure are in good agreement with the corresponding simulations (Fig. 4, E to H). In addition, the experimental results for $d = -40$ μm and $s = 15$, 25, 35, and 45 μm (Fig. 4, I to L) are also consistent with the corresponding simulations (Fig. 4, M to P). As indicated by the color scale, the changes of the surface amplitudes are in accordance with those in Fig. 3 (C and F). Therefore, the modulation capability of the EIT driven SPs is confirmed.

DISCUSSION

The preceding analysis shows that the excitation of SRSR resonance arises from the near-field coupling with BSSR. Therefore, it can be understood that the SPs to the SRSR (right) side are gradually converted to the SPs propagating to the top and bottom sides. Such a behavior is further applied to control the focusing direction of the SPs, which is fascinating in many applications. The schematic diagram is illustrated in Fig. 5A. Two series of concentric circles centered respectively at the blue and red elliptical points intersect with each other. The radial difference between the neighboring concentric circles is 400 μm. The structural unit cells are placed right at the intersection points, as indicated by the brown points. When there are only the BSSRs (Fig. 5B), a strong focusing behavior is observed at the red central point, and a diverging behavior is observed at the opposite (left) side. However, the SPs at the top and bottom sides are much weaker because of the fact that the SP excitation along the long-axial direction of BSSR is weak. Figure 5 (C and D) illustrates the results when SRSR is placed at the right and left sides of BSSR, respectively. For the first case, part of the focused SP toward the right side in the original configuration (Fig. 5B) is now redirected to the focused SP propagating downward toward the blue point and the diverged SP propagating upward (Fig. 5C). Whereas for the second case, most of the energy in the diverging SP toward the left side in the original configuration (Fig. 5B) is redirected into those two directions (focusing downward and diverging upward) (Fig. 5D). The energy redirection in both cases is indicated by the corresponding white arrows and the amplitude changes. This method also provides a route for fully using the energy of the excited SPs where the part of the concomitantly diverging SPs is usually useless in many cases. Here, the focusing area is a line segment rather than a point-like spot due to the fact that only parts of the circles are applied to excite the SPs. The focusing resolutions of all the focus points are around $0.65\lambda_{SP}$, with λ_{SP} (≈400 μm) denoting the SP wavelength at 0.75 THz.

It should be noted that the intensity of the SPs along the y direction cannot be enhanced but will decrease to zero if another SRSR is placed symmetrically at the other side of BSSR. Owing to the resonant feature of BSSR, it will excite SRSRs at its two sides with an exact π phase difference. Although the SPs along both the $+x$ and $-x$ directions will be suppressed simultaneously, the excited SPs by these two SRSRs will cancel each other out (see fig. S5). Furthermore, because the coupling mechanism of the EIT in metamaterials is universal, the proposed method of asymmetric excitation of SPs is also applicable to other spectral regimes. As an example, we theoretically investigate a metasurface that is made up of similar BSSRs and SRSRs at infrared frequencies and achieve results comparable to those in Figs. 2 and 3 (see fig. S6).

In summary, SP excitation via the EIT coupling mechanism is proposed in a metasurface containing two coupled hole-type resonators. Through manipulating the near-field coupling, the intensity of the excited SPs can be effectively controlled. The proposed approach is further applied to control the SP focusing by properly engineering the arrangement of the unit cells. Our experimental findings provide the possibility of developing a wide range of SP-based applications.

MATERIALS AND METHODS

Experimental design

All the metasurfaces were characterized by using a terahertz time-domain near-field scanning system that we recently developed. Different from a traditional terahertz time-domain system, here, the terahertz detector was a near-field photoconductive antenna-based probe (Protemics GmbH). To allow the movements of the probe, the detection beam of the system was coupled to a 2-m-long optical fiber. Before that, a pre-dispersion–compensation grating pair was used to suppress

pulse stretching in the fiber. Then, the probe was fixed onto a 2D electrically controlled translation stage. In the measurements, the terahertz probe was placed approximately 50 μm above the sample surface. The entire 2D scanning range was 8×8 mm^2 for the metasurface with 8×8 unit cells and 7.8×7.8 mm^2 for the SP focusing metasurfaces.

Numerical simulations

The numerical simulations were carried out using the finite-element time-domain solver of the CST Microwave Studio. The entire simulation area was 8×8 mm^2. The structure contained 8×8 unit cells located at the center of the simulation area. Open-boundary conditions were applied in both the x and y directions. The incident wave was x-polarized and normally illuminating on the metasurface from the substrate side. The SP spectra were extracted by setting field probes at the corresponding positions, whereas the field distributions of the SP were mapped by defining electric field monitors at 0.75 THz. The simulated results were also obtained at 50 μm above the metasurface on the air side.

SUPPLEMENTARY MATERIALS

Supplementary material for this article is available at http://advances.sciencemag.org/cgi/content/full/2/2/e1501142/DC1

Fig. S1. Simulated SP spectrum and field distribution of the BSSR array.
Fig. S2. Simulated E_z and H_x field distributions of the BSSR and BSSR + SRSR.
Fig. S3. Simulated spectrum variations with different values of d and s.
Fig. S4. Schematics to describe the coupling mechanism using complementary structures.
Fig. S5. Simulated SP spectrum and field distribution of the BSSR + 2 × SRSR array.
Fig. S6. Simulated SP field distributions and spectra of similar metasurfaces in the infrared regime.
Note S1. Coupled Lorentzian oscillator model.

REFERENCES AND NOTES

1. S. E. Harris, Electromagnetically induced transparency. *Phys. Today* **50**, 36 (1997).
2. S. Zhang, D. A. Genov, Y. Wang, M. Liu, X. Zhang, Plasmon-induced transparency in metamaterials. *Phys. Rev. Lett.* **101**, 047401 (2008).
3. N. Papasimakis, V. A. Fedotov, N. I. Zheludev, S. L. Prosvirnin, Metamaterial analog of electromagnetically induced transparency. *Phys. Rev. Lett.* **101**, 253903 (2008).
4. P. Tassin, L. Zhang, T. Koschny, E. N. Economou, C. M. Soukoulis, Low-loss metamaterials based on classical electromagnetically induced transparency. *Phys. Rev. Lett.* **102**, 053901 (2009).
5. R. Singh, C. Rockstuhl, F. Lederer, W. Zhang, Coupling between a dark and a bright eigenmode in a terahertz metamaterial. *Phys. Rev. B* **79**, 085111 (2009).
6. N. Liu, L. Langguth, T. Weiss, J. Kästel, M. Fleischhauer, T. Pfau, H. Giessen, Plasmonic analogue of electromagnetically induced transparency at the Drude damping limit. *Nat. Mater.* **8**, 758–762 (2009).
7. Z.-G. Dong, H. Liu, M.-X. Xu, T. Li, S.-M. Wang, J.-X. Cao, S.-N. Zhu, X. Zhang, Role of asymmetric environment on the dark mode excitation in metamaterial analogue of electromagnetically-induced transparency. *Opt. Express* **18**, 22412–22417 (2010).
8. X. Liu, J. Gu, R. Singh, Y. Ma, J. Zhu, Z. Tian, M. He, J. Han, W. Zhang, Electromagnetically induced transparency in terahertz plasmonic metamaterials via dual excitation pathways of the dark mode. *Appl. Phys. Lett.* **100**, 131101 (2012).
9. J. Gu, R. Singh, X. Liu, X. Zhang, Y. Ma, S. Zhang, S. A. Maier, Z. Tian, A. K. Azad, H.-T. Chen, A. J. Taylor, J. Han, W. Zhang, Active control of electromagnetically induced transparency analogue in terahertz metamaterials. *Nat. Commun.* **3**, 1151 (2012).
10. X. Zhang, Q. Li, W. Cao, J. Gu, R. Singh, Z. Tian, J. Han, W. Zhang, Polarization-independent plasmon-induced transparency in a fourfold symmetric terahertz metamaterial. *IEEE J. Sel. Top. Quant. Electron.* **19**, 8400707 (2013).
11. W. Cao, R. Singh, C. Zhang, J. Han, M. Tonouchi, W. Zhang, Plasmon-induced transparency in metamaterials: Active near field coupling between bright superconducting and dark metallic mode resonators. *Appl. Phys. Lett.* **103**, 101106 (2013).
12. Y. Yang, I. I. Kravchenko, D. P. Briggs, J. Valentine, All-dielectric metasurface analogue of electromagnetically induced transparency. *Nat. Commun.* **5**, 5753 (2014).
13. U. Fano, Effects of configuration interaction on intensities and phase shifts. *Phys. Rev.* **124**, 1866–1878 (1961).
14. N. Verellen, Y. Sonnefraud, H. Sobhani, F. Hao, V. V. Moshchalkov, P. V. Dorpe, P. Nordlander, S. A. Maier, Fano resonances in individual coherent plasmonic nanocavities. *Nano Lett.* **9**, 1663–1667 (2009).
15. B. Luk'yanchuk, N. I. Zheludev, S. A. Maier, N. J. Halas, P. Nordlander, H. Giessen, C. T. Chong, The Fano resonance in plasmonic nanostructures and metamaterials. *Nat. Mater.* **9**, 707–715 (2010).
16. R. Singh, I. A. I. Al-Naib, Y. Yang, D. R. Chowdhury, W. Cao, C. Rockstuhl, T. Ozaki, R. Morandotti, W. Zhang, Observing metamaterial induced transparency in individual Fano resonators with broken symmetry. *Appl. Phys. Lett.* **99**, 201107 (2011).
17. N. Liu, T. Weiss, M. Mesch, L. Langguth, U. Eigenthaler, M. Hirscher, C. Sönnichsen, H. Giessen, Planar metamaterial analogue of electromagnetically induced transparency for plasmonic sensing. *Nano Lett.* **10**, 1103–1107 (2010).
18. C.-Y. Chen, I.-W. Un, N.-H. Tai, T.-J. Yen, Asymmetric coupling between subradiant and superradiant plasmonic resonances and its enhanced sensing performance. *Opt. Express* **17**, 15372–15380 (2009).
19. Z.-G. Dong, H. Liu, J.-X. Cao, T. Li, S.-M. Wang, S.-N. Zhu, X. Zhang, Enhanced sensing performance by the plasmonic analog of electromagnetically induced transparency in active metamaterials. *Appl. Phys. Lett.* **97**, 114101 (2010).
20. Y. Sun, Y.-w. Tong, C.-h. Xue, Y.-q. Ding, Y.-h. Li, H. Jiang, H. Chen, Electromagnetic diode based on nonlinear electromagnetically induced transparency in metamaterials. *Appl. Phys. Lett.* **103**, 091904 (2013).
21. R. D. Kekatpure, E. S. Barnard, W. Cai, M. L. Brongersma, Phase-coupled plasmon-induced transparency. *Phys. Rev. Lett.* **104**, 243902 (2010).
22. Z. Han, S. I. Bozhevolnyi, Plasmon-induced transparency with detuned ultracompact Fabry-Perot resonators in integrated plasmonic devices. *Opt. Express* **19**, 3251–3257 (2011).
23. Y. Huang, C. Min, G. Veronis, Subwavelength slow-light waveguides based on a plasmonic analogue of electromagnetically induced transparency. *Appl. Phys. Lett.* **99**, 143117 (2011).
24. S. A. Maier, Plasmonics: Fundamentals and Applications (Springer-Verlag, New York, 2007).
25. N. Yu, P. Genevet, M. A. Kats, F. Aieta, J.-P. Tetienne, F. Capasso, Z. Gaburro, Light propagation with phase discontinuities: Generalized laws of reflection and refraction. *Science* **334**, 333–337 (2011).
26. X. Ni, N. K. Emani, A. V. Kildishev, A. Boltasseva, V. M. Shalaev, Broadband light bending with plasmonic nanoantennas. *Science* **335**, 427–427 (2012).
27. L. Huang, X. Chen, H. Mühlenbernd, G. Li, B. Bai, Q. Tan, G. Jin, T. Zentgraf, S. Zhang, Dispersionless phase discontinuities for controlling light propagation. *Nano Lett.* **12**, 5750–5755 (2012).
28. X. Chen, L. Huang, H. Mühlenbernd, G. Li, B. Bai, Q. Tan, G. Jin, C.-W. Qiu, S. Zhang, T. Zentgraf, Dual-polarity plasmonic metalens for visible light. *Nat. Commun.* **3**, 1198 (2012).
29. F. Aieta, P. Genevet, M. A. Kats, N. Yu, R. Blanchard, Z. Gaburro, F. Capasso, Aberration-free ultrathin flat lenses and axicons at telecom wavelengths based on plasmonic metasurfaces. *Nano Lett.* **12**, 4932–4936 (2012).
30. S. Sun, K.-Y. Yang, C.-M. Wang, T.-K. Juan, W. T. Chen, C. Y. Liao, Q. He, S. Xiao, W.-T. Kung, G.-Y. Guo, L. Zhou, D. P. Tsai, High-efficiency broadband anomalous reflection by gradient meta-surfaces. *Nano Lett.* **12**, 6223–6229 (2012).
31. X. Zhang, Z. Tian, W. Yue, J. Gu, S. Zhang, J. Han, W. Zhang, Broadband terahertz wave deflection based on C-shape complex metamaterials with phase discontinuities. *Adv. Mater.* **25**, 4567–4572 (2013).
32. Z. Li, E. Palacios, S. Butun, K. Aydin, Visible-frequency metasurfaces for broadband anomalous reflection and high-efficiency spectrum splitting. *Nano Lett.* **15**, 1615–1621 (2015).
33. S. Sun, Q. He, S. Xiao, Q. Xu, X. Li, L. Zhou, Gradient-index meta-surfaces as a bridge linking propagating waves and surface waves. *Nat. Mater.* **11**, 426–431 (2012).
34. L. Huang, X. Chen, B. Bai, Q. Tan, G. Jin, T. Zentgraf, S. Zhang, Helicity dependent directional surface plasmon polariton excitation using a metasurface with interfacial phase discontinuity. *Light: Sci. Appl.* **2**, e70 (2013).
35. A. Pors, M. G. Nielsen, T. Bernardin, J.-C. Weeber, S. I. Bozhevolnyi, Efficient unidirectional polarization-controlled excitation of surface plasmon polaritons. *Light: Sci. Appl.* **3**, e197 (2014).
36. F. López-Tejeira, S. G. Rodrigo, L. Martín-Moreno, F. J. García-Vidal, E. Devaux, T. W. Ebbesen, J. R. Krenn, I. P. Radko, S. I. Bozhevolnyi, M. U. González, J. C. Weeber, A. Dereux, Efficient unidirectional nanoslit couplers for surface plasmons. *Nat. Phys.* **3**, 324–328 (2007).
37. S. B. Choi, D. J. Park, Y. K. Jeong, Y. C. Yun, M. S. Jeong, C. C. Byeon, J. H. Kang, Q.-H. Park, D. S. Kim, Directional control of surface plasmon polariton waves propagating through an asymmetric Bragg resonator. *Appl. Phys. Lett.* **94**, 063115 (2009).
38. J. S. Q. Liu, R. A. Pala, F. Afshinmanesh, W. Cai, M. L. Brongersma, A submicron plasmonic dichroic splitter. *Nat. Commun.* **2**, 525 (2011).

39. Y. Liu, S. Palomba, Y. Park, T. Zentgraf, X. Yin, X. Zhang, Compact magnetic antennas for directional excitation of surface plasmons. *Nano Lett.* **12**, 4853–4858 (2012).
40. J. Lin, J. P. B. Mueller, Q. Wang, G. Yuan, N. Antoniou, X.-C. Yuan, F. Capasso, Polarization-controlled tunable directional coupling of surface plasmon polaritons. *Science* **340**, 331–334 (2013).
41. F. J. Rodríguez-Fortuño, G. Marino, P. Ginzburg, D. O'Connor, A. Martínez, G. A. Wurtz, A. V. Zayats, Near-field interference for the unidirectional excitation of electromagnetic guided modes. *Science* **340**, 328–330 (2013).
42. T. Coenen, F. B. Arango, A. F. Koenderink, A. Polman, Directional emission from a single plasmonic scatterer. *Nat. Commun.* **5**, 3250 (2014).
43. T. Tanemura, K. C. Balram, D.-S. Ly-Gagnon, P. Wahl, J. S. White, M. L. Brongersma, D. A. B. Miller, Multiple-wavelength focusing of surface plasmons with a nonperiodic nanoslit coupler. *Nano Lett.* **11**, 2693–2698 (2011).
44. D. Wintz, P. Genevet, A. Ambrosio, A. Woolf, F. Capasso, Holographic metalens for switchable focusing of surface plasmons. *Nano Lett.* **15**, 3585–3589 (2015).
45. J. Saxler, J. G. Rivas, C. Janke, H. P. M. Pellemans, P. H. Bolívar, H. Kurz, Time-domain measurements of surface plasmon polaritons in the terahertz frequency range. *Phys. Rev. B.* **69**, 155427 (2004).
46. K. Wang, D. M. Mittleman, Metal wires for terahertz wave guiding. *Nature* **432**, 376–379 (2004).
47. T.-I. Jeon, D. Grischkowsky, THz Zenneck surface wave (THz surface plasmon) propagation on a metal sheet. *Appl. Phys. Lett.* **88**, 061113 (2006).
48. J. Han, X. Lu, W. Zhang, Terahertz transmission in subwavelength holes of asymmetric metal-dielectric interfaces: The effect of a dielectric layer. *J. Appl. Phys.* **103**, 033108 (2008).
49. A. Rusina, M. Durach, K. A. Nelson, M. I. Stockman, Nanoconcentration of terahertz radiation in plasmonic waveguides. *Opt. Express* **16**, 18576–18589 (2008).
50. Q. Wang, X. Zhang, Y. Xu, Z. Tian, J. Gu, W. Yue, S. Shuang, J. Han, W. Zhang, A broadband metasurface-based terahertz flat-lens array. *Adv. Opt. Mater.* **3**, 779–785 (2015).
51. F. Falcone, T. Lopetegi, M. A. G. Laso, J. D. Baena, J. Bonache, M. Beruete, R. Marqués, F. Martín, M. Sorolla, Babinet principle applied to the design of metasurfaces and metamaterials. *Phys. Rev. Lett.* **93**, 197401 (2004).
52. T. Zentgraf, T. P. Meyrath, A. Seidel, S. Kaiser, H. Giessen, C. Rockstuhl, F. Lederer, Babinet's principle for optical frequency metamaterials and nanoantennas. *Phys. Rev. B.* **76**, 033407 (2007).
53. H.-T. Chen, J. F. O'Hara, A. J. Tayloy, R. D. Averitt, C. Highstrete, M. Lee, W. J. Padilla, Complementary planar terahertz metamaterials. *Opt. Express* **15**, 1084–1095 (2007).

Acknowledgments

Funding: This work was supported by the Cooperative Innovation Center of Terahertz Science, the National Key Basic Research Program of China (grant no. 2014CB339800), the National Science Foundation of China (grant nos. 61138001, 61422509, 61427814, and 61420106006), the Program for Changjiang Scholars and Innovative Research Team in University (grant no. IRT13033), the Major National Development Project of Scientific Instruments and Equipment (grant no. 2011YQ150021), the Specialized Research Fund for the Doctoral Program of Higher Education (grant no. 20110032120058), and the U.S. NSF (grant no. ECCS-1232081). **Author contributions:** XQ.Z. and Q.X. proposed the mechanism of asymmetric excitation of SPs and conducted the experimental design; XQ.Z. completed numerical simulations; XQ.Z. fabricated the metasurface samples; XQ.Z. Q.X., and Y.X. performed all the measurements; XQ.Z. Q.X., and Q.L. developed the analytical model and discussed the comparisons between simulations and experiments; XQ.Z., Q.X., Q.L., Y.X., Z.T., J.G., C.O., Y.L., S.Z., XX.Z., J.H., and W.Z. analyzed the measured data; and S.Z., J.H., and W.Z. supervised the theory and measurements. All the authors discussed the results and contributed to the writing of the manuscript. **Competing interests:** The authors declare that they have no competing interests. **Data and materials availability:** All data needed to evaluate the conclusions are present in the paper and the Supplementary Materials. Additional data are available from the authors upon request.

Submitted 22 August 2015
Accepted 13 December 2015
Published 19 February 2016
10.1126/sciadv.1501142

Citation: X. Zhang, Q. Xu, Q. Li, Y. Xu, J. Gu, Z. Tian, C. Ouyang, Y. Liu, S. Zhang, X. Zhang, J. Han, W. Zhang, Asymmetric excitation of surface plasmons by dark mode coupling. *Sci. Adv.* **2**, e1501142 (2016).

Science Advances

Asymmetric excitation of surface plasmons by dark mode coupling

Xueqian Zhang, Quan Xu, Quan Li, Yuehong Xu, Jianqiang Gu, Zhen Tian, Chunmei Ouyang, Yongmin Liu, Shuang Zhang, Xixiang Zhang, Jiaguang Han and Weili Zhang

Sci Adv **2** (2), e1501142.
DOI: 10.1126/sciadv.1501142